Magnetic Resonance Imaging 83 (2021) 152–159

Contents lists available at ScienceDirect

Magnetic Resonance Imaging

journal homepage: www.elsevier.com/locate/mri

Original Contribution

Quantitative diffusion-weighted imaging and dynamic contrast-enhanced MR imaging for assessment of tumor aggressiveness in prostate cancer at 3T

Takeshi Fukunaga [a,*], Tsutomu Tamada [a], Naoki Kanomata [b], Mitsuru Takeuchi [c], Yu Ueda [d], Yoshiyuki Miyaji [e], Ayumu Kido [a], Akira Yamamoto [a], Teruki Sone [a]

[a] Department of Radiology, Kawasaki Medical School, 577 Matsushima, Kurashiki-city, Okayama 701-0192, Japan
[b] Department of Pathology, Kawasaki Medical School, 577 Matsushima, Kurashiki-city, Okayama 701-0192, Japan
[c] Department of Radiology, Radiolonet Tokai, Asaoka-cho 3-86-2, Chikusa-ku, Nagoya-city, Aichi 464-0811, Japan
[d] Philips Japan, Konan 2-13-37, Minato-ku, Tokyo 108-8507, Japan
[e] Department of Urology, Kawasaki Medical School, 577 Matsushima, Kurashiki-city, Okayama 701-0192, Japan

ARTICLE INFO

Keywords:
Prostate cancer
MR imaging
Diffusion-weighted imaging
Dynamic contrast-enhanced MR imaging
Tumor aggressiveness
Apparent diffusion coefficient

ABSTRACT

Purpose: To compare diffusion-weighted imaging (DWI) and dynamic contrast-enhanced MR imaging (DCE-MRI) for characterization of prostate cancer (PC).

Methods: 104 PC patients who underwent prostate multiparametric MRI at 3T including DWI and DCE-MRI before MRI-guided biopsy or radical prostatectomy. Apparent diffusion coefficient (ADC) with histogram analysis (mean, 0–25th percentile, skewness, and kurtosis), intravoxel incoherent motion model including *D* and *f*; stretched exponential model including distributed diffusion coefficient (*DDC*) and *α*; and permeability parameters including K^{trans}, K_{ep}, and V_e were obtained from a region of interest placed on the dominant tumor of each patient.

Results: ADC_{mean}, $ADC_{0–25}$, *D*, *DDC*, and V_e were significantly lower and K_{ep} was significantly higher in GS $\geq 3+4$ tumors ($n = 89$) than in GS $= 3+3$ tumors ($n = 15$), and also in GS $\geq 4+3$ tumors ($n = 57$) than in GS $\leq 3+4$ tumors ($n = 47$) ($P < 0.001$ to $P = 0.040$). *f* was significantly lower in GS $\geq 4+3$ tumors than in GS $\leq 3+4$ tumors ($P = 0.022$), but there was no significant difference between GS $= 3+3$ tumors and GS $\geq 3+4$ tumors, or between the remaining metrics in both comparisons. In metrics with area under the curve (AUC) >0.80, there was a significant difference in AUC between $ADC_{0–25}$ and *D*, and *DDC* for separating GS $\leq 3+4$ tumors from GS $\geq 4+3$ tumors (P = 0.040 and P = 0.022, respectively). There were no significant differences between metrics with AUC > 0.80 for separating GS $= 3+3$ tumors from GS $\geq 3+4$ tumors. $ADC_{0–25}$ had the highest correlation with Gleason grade ($\rho = -0.625$, $P < 0.001$).

Conclusions: DWI and DCE-MRI showed no apparent clinical superiority of non-Gaussian models or permeability MRI over the mono-exponential model for assessment of tumor aggressiveness in PC.

Abbreviations: DWI, diffusion-weighted imaging; DCE-MRI, dynamic contrast-enhanced MR imaging; PC, prostate cancer; ADC, apparent diffusion coefficient; *DDC*, distributed diffusion coefficient; AUC, area under the curve; cs, clinically significant; cis, clinically insignificant; PSA, prostate-specific antigen; TRUS, transrectal ultrasonography; GS, Gleason score; IVIM, intravoxel incoherent motion; mpMRI, multiparametric MRI; MRGB, MRI-guided prostate biopsy; MRFGB, MRI-TRUS fusion-guided biopsy; T2WI, T2-weighted imaging; 3D, three-dimensional; PI-RADS v2, Prostate Imaging Reporting and Data System Version 2; TSE, turbo spin echo; TR, repetition time; TE, echo time; FOV, field of view; MPG, motion-probing gradient; FFE, fast field echo; ISP, IntelliSpace Portal; 2D, two-dimensional; ROI, region of interest; ROC, receiver-operating characteristic; GG, Gleason grade; PSAD, PSA density; PCA3, prostate cancer antigen 3; PHI, Prostate Health Index; 4 K, four kallikrein; VOI, volume of interest.

* Corresponding author.
E-mail addresses: kcnfm627@yahoo.co.jp (T. Fukunaga), ttamada@med.kawasaki-m.ac.jp (T. Tamada), kanomnao@luke.ac.jp (N. Kanomata), yu.ueda@philips.com (Y. Ueda), miyaji@med.kawasaki-m.ac.jp (Y. Miyaji), a-k.24@med.kawasaki-m.ac.jp (A. Kido), jiro@med.kawasaki-m.ac.jp (A. Yamamoto), tsone@med.kawasaki-m.ac.jp (T. Sone).

https://doi.org/10.1016/j.mri.2021.08.009
Received 5 October 2020; Received in revised form 13 July 2021; Accepted 23 August 2021
Available online 25 August 2021

1. Introduction

Prostate cancer (PC) can be classified as a clinically significant (cs) tumor for which curative therapies such as radical prostatectomy are indicated, and also as a clinically insignificant (cis) tumor for which active surveillance of serum Prostate-specific antigen (PSA) is indicated. Therefore, accurate pre-treatment risk stratification using tumor size, tumor aggressiveness, and extracapsular extension is essential in determining the treatment strategy for PC. Systematic transrectal ultrasonography (TRUS)-guided prostate biopsy, which is a standard method for histopathological evaluation of PC before treatment in patients with elevated PSA levels currently plays an important role in discriminating csPC from cisPC. However, this biopsy has several limitations, including the inability to accurately visualize the PC on TRUS, and underestimation of indicators of tumor aggressiveness such as the Gleason score (GS) and the tumor size of PC [1,2].

Previous studies that assessed tumor aggressiveness have shown that the apparent diffusion coefficient (ADC) calculated using an mono-exponential model from DWI acquisitions could discriminate between low-risk and moderate- to high-risk PC [3]. In addition, several studies have reported that ADC parameters such as the 0–25th percentile, derived from ADC histogram analysis, have higher discrimination ability for tumor aggressiveness compared with the mean ADC value [4]. In PC tissues, however, water diffusion is obstructed by microstructural complexity, so a more complex non-Gaussian model may better characterize the diffusion behavior [5]. The non-Gaussian behavior of diffusion can be investigated using DWI with high b-values and a relatively large number of b-values. Recent hardware and software advances have enabled the use of higher b-values such as 2000 s/mm^2 and advanced DWI acquisition and modeling methods [6].

As non-Gaussian models that use a large number of b-values ranging from very low to high, the intravoxel incoherent motion (IVIM) model (a bi-exponential fitting model that evaluates extravascular molecular diffusion and the microcirculation of blood within the capillaries separately) and the stretched exponential model (which reflects the deviation of the curve from mono-exponential behavior) may be more reliable and reproducible methods for assessing tumor aggressiveness compared with the mono-exponential model [7–9]. Previous studies also have shown that DCE-MRI with permeability MRI, which provides information about angiogenesis, has potential for assessing PC aggressiveness [10,11]. However, few studies have used both DWI and DCE-MRI for assessment of PC aggressiveness at 3T [12]. Thus, the purpose of this study was to compare DWI with ADC histogram analysis, IVIM, and stretched exponential model and DCE-MRI with permeability MRI for characterization of PC.

2. Materials and methods

2.1. Study population

Our Institutional Review Board approved this retrospective study and waived the need for informed consent. Between April 2017 and February 2019, 122 consecutive patients with pathologically confirmed PC underwent 3T prostate multiparametric MRI (mpMRI) prior to MRI-guided prostate biopsy (MRGB: MRI-TRUS fusion-guided biopsy (MRFGB) or TRUS-guided cognitive-targeted biopsy) for lesions suspicious for PC on mpMRI. Eighteen patients were removed from the study based on the following exclusion criteria: small PC lesions that were invisible on MRI (n = 12) and incomplete MRI examination (n = 6). Thus, 104 patients (age range, 57–87 years; mean age, 71 years) with PC lesions visible on MRI were included in the study. The median PSA level at the time of the initial MRI was 7.83 ng/mL (PSA range, 1.33–2860.30 ng/mL). The mean interval between the MRI examination and MRGB was 45 ± 38 days (range, 0–153 days; median, 35 days). All patients underwent mpMRI including T2-weighted imaging (T2WI), DWI, and DCE-MRI, and 92/104 patients underwent mpMRI (T2WI and DWI) without DCE-MRI. No patient had undergone any therapy for PC at the time of the MRI examination, and 30/104 patients underwent radical prostatectomy after MRGB.

2.2. MRGB

Final pathological diagnosis was determined by TRUS-guided cognitive-targeted biopsy in 25 patients, MRFGB in 49 patients, and radical prostatectomy in 30 patients. In cognitive-targeted biopsy, the location of a lesion detected on MRI is estimated and the target is mentally transferred to the TRUS image during TRUS-guided biopsy [13]. All MRFGB procedures were performed using the UroStation system (Koelis; Grenoble, France) with elastic image fusion, real-time three-dimensional (3D) tracking technology, and a computer workstation (Koelis) for segmentation of the prostate. The MRFGB procedure is described in detail in our previous study [14]. MRGB was performed for lesions with PI-RADS categories of 3 to 5 (Prostate Imaging Reporting and Data System Version 2 (PI-RADS v2)) and for highly suspicious lesions according to conventional overall mpMRI assessment [15]. At least two cores were obtained for each MRI-targeted lesion.

2.3. Histopathologic examination

The MRGB specimens underwent hematoxylin and eosin staining. Radical prostatectomy specimens underwent standard step sections at intervals of 4–6 mm, with subsequent hematoxylin and eosin staining. A uropathologist with 23 years of experience who was blinded to the MRI findings recorded the presence or absence of PC and tumor Gleason score (GS) for biopsy specimens; and recorded tumor location, the GS of all tumor foci, and the locations of extraprostatic extension on a standardized diagram of the prostate for prostatectomy specimens. GS was evaluated according to the 2014 International Society of Urological Pathology Modified Gleason Grading System [16].

2.4. MR imaging technique

The mpMRI examinations of the prostate were performed on a 3T scanner with a 32-channel phased-array coil (Ingenia 3.0T CX Quasar Dual; Philips Healthcare, Best, The Netherlands). All examinations were performed with patients in the fasting condition, and all patients received intramuscular buscopan or glucagon to reduce intestinal peristalsis.

The following pulse sequences were used: axial turbo spin echo (TSE) T2WI (repetition time (TR)/echo time (TE) 7257/95 ms; slice thickness 3 mm; no intersection gap; field of view (FOV) 200 × 200 mm, matrix 352 × 277, in-plane resolution 0.57 × 0.72 mm^2, parallel imaging factor 1.4), coronal TSE T2WI (TR/TE 5730/95 ms; slice thickness 4 mm; no intersection gap; FOV 200 × 200 mm, matrix 272 × 187, in-plane resolution 0.74 × 1.07 mm^2, parallel imaging factor 1.8), and axial fat-suppressed single-shot spin echo echo-planar DWI (TR/TE 6000/70 ms; slice thickness 3 mm; no intersection gap; FOV 300 × 300 mm, matrix 112 × 112, in-plane resolution 2.68 × 2.68 mm^2, parallel imaging factor 2; b-values 0, 30, 50, 100, 200, 500, 1000, and 2000 s/mm^2). DWI was acquired with motion-probing gradient (MPG) pulses applied sequentially along the three orthogonal orientations following acquisition at eight b-values of 0, 30, 50, 100, 200, 500, 1000, and 2000 s/mm^2. ADC maps were constructed by calculating the ADC in each pixel of each slice. In addition, data acquisition for DCE-MRI began simultaneously with the start of intravenous injection of gadolinium-based contrast medium at 0.1 mmol/kg body weight at a rate of 1.5 mL/s (gadobutrol (Gadovist); Bayer Schering Pharma, Osaka, Japan) via power injector, followed by a 30 mL saline flush at the same rate as the contrast medium injection. Multiphase DCE-MR images were obtained every 7 s for 182 s (26 phases) (non-fat suppressed three-dimensional (3D) fast field echo (FFE) (TR, 3.1 ms; TE, 1.45 ms; slice thickness, 3.5 mm; no interslice gap; FOV, 250 × 250 mm; matrix 192 × 144; in-plane resolution, 1.30 × 1.74 mm^2; parallel imaging factor, 1.7)),

without breath-holding. Axial T1WI and 3D T2WI were also performed, but not assessed in the present study.

2.5. Image analysis

Prior to quantitative assessment, a fellowship-trained radiologist with 21 years of experience in prostate MR imaging (T.T.) determined a single dominant target lesion per patient for image analysis using the mpMR images in conjunction with the pathologic reports with maps. The mpMRI assessment was performed using a standard picture archiving and communication system (Synapse EX, Fujifilm Corporation, Japan). When a patient had multiple PC lesions, the index lesion was a tumor with a diameter of at least 5 mm and highest GS. If there were multiple lesions with highest GS, the largest of these was selected. The biopsy GS was adopted for patients who underwent only MRGB ($n = 74$; cognitive biopsy in 25 and MRFGB in 49) and the prostatectomy GS was adopted for patients who underwent radical prostatectomy ($n = 30$). If the GS differed among MRGB specimens of the same target lesion, the highest GS was used for analysis. In quantitative analysis of each patient's dominant lesion, matching between the mpMR images and the index histologic lesion for MRGB was performed using a PowerPoint file that showed the mpMR images of the targeted lesion used for the MRGB and the pathological report. Matching for patients with prostatectomy was performed considering the size of the lesion and its overall position in the craniocaudal, anteroposterior, and left–right planes on both the pathologic maps and the mpMR images. For each patient, the radiologist created a folder containing a DWI image, an ADC map, and a DCE-MRI image showing the target lesion, for use when performing the quantitative analysis.

The quantitative DWI and DCE-MRI measurements were performed in consensus by two fellowship-trained radiologists with 21 years and 3 years of experience in prostate MR imaging (T.F. and T.T., respectively)

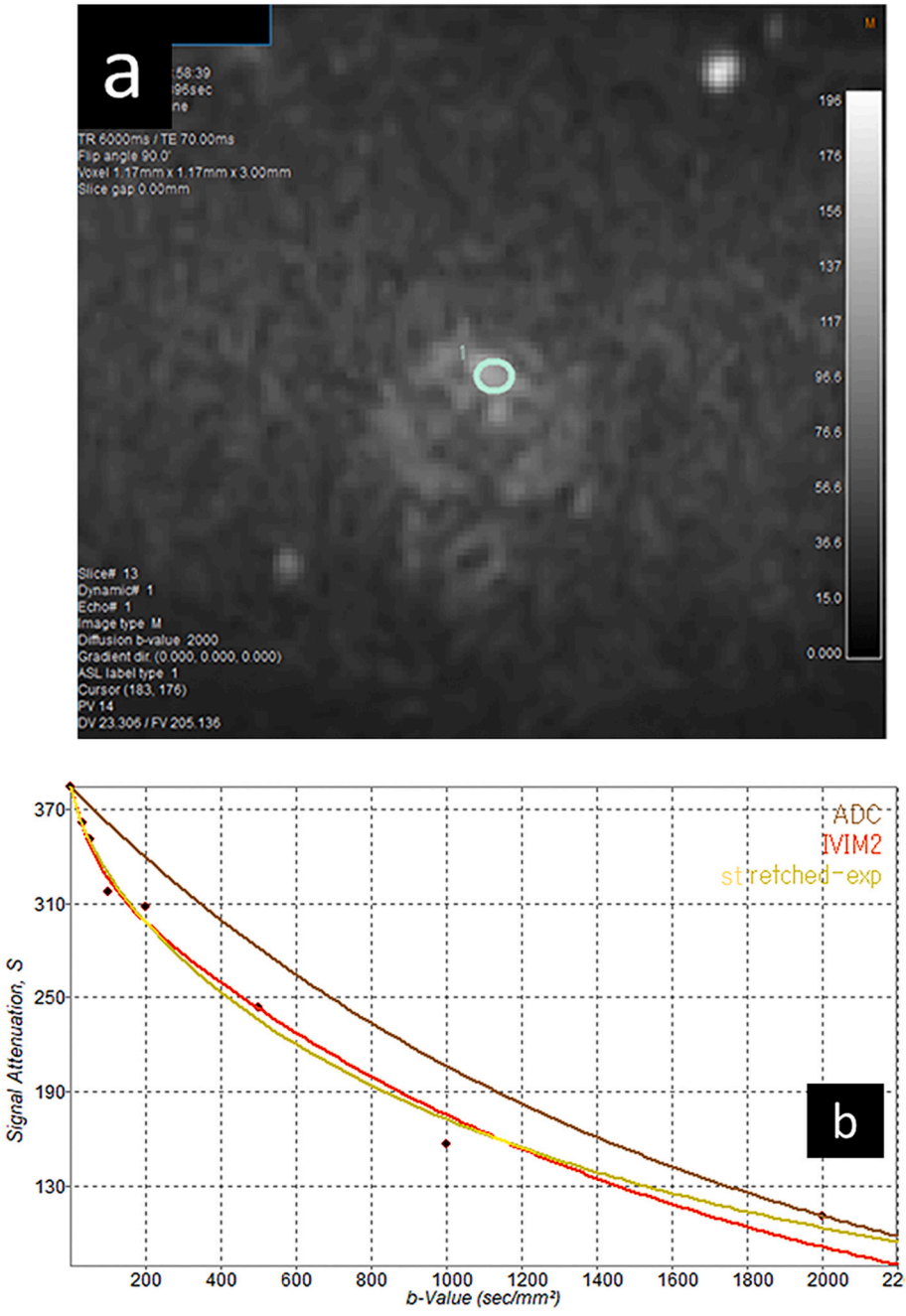

Fig. 1. Representative example of quantitative DWI analysis (ADC with histogram analysis (mean, 0–25th percentile, skewness, and kurtosis), intravoxel incoherent motion model (IVIM) including *D* and *f*, and stretched exponential model including *DDC* and α of a 71-year-old man with prostate cancer in the left transitional zone (circle), using dedicated software (IVIM 2018). a: DWI shows moderate hyperintensity within a circular ROI in the left transition zone. b: Fitting curves of mono-exponential ADC, IVIM, and stretched exponential model. DWI: diffusion-weighted imaging; ADC: apparent diffusion coefficient; *DDC*; distributed diffusion coefficient; ROI: region of interest.

using dedicated post-processing software (IVIM 2018; Philips Healthcare) for ADC with histogram analysis, IVIM, and stretched exponential model and a dedicated post-processing workstation (IntelliSpace Portal (ISP); Philips Healthcare) for blood vessel permeability parameters. The radiologists traced a two-dimensional (2D) region of interest (ROI) encompassing the entire target lesion on a single slice of DWI with b = 2000 s/mm^2 on IVIM 2018 software or on a single slice of DCE-MRI, on an ISP workstation with reference to the MR images in the folder prepared in advance (Figs. 1, 2). Each ROI was placed ellipse or freehand and was as large as possible. All of the PC lesions could be recognized as visible tumor on DWI. If the target lesion could not be visually identified on DCE-MRI, a ROI of visible tumor on the DWI image was copied and pasted to the corresponding DCE-MRI image. The following were extracted from the ROI: ADC histogram analysis including the mean (ADC_{mean}), 0–25th percentile ($ADC_{0–25}$), skewness ($ADC_{skewness}$ as a measure of the asymmetry of the distribution), and kurtosis ($ADC_{kurtosis}$ as a measure of the sharpness of the peak of the distribution); IVIM including *D* (diffusion coefficient of slow decay) and *f* (perfusion fraction of fast decay); stretched model including distributed diffusion coefficient (*DDC*) and *α*; and blood vessel permeability parameters including K^{trans}, K_{ep}, and V_e.

ADC was calculated for a pair of b-values (0 and 2000 s/mm^2) by mono-exponential fitting with the following equation:

$$S_b = S_0 \cdot exp.\{-b\mathrm{ADC}\} \quad (1)$$

In addition, we analyzed the IVIM using bi-exponential fitting with eight b-values with the following equation:

$$S_b = S_0\{F \bullet \exp(-\mathrm{bD}^*) + (1-\mathrm{F}) \bullet \exp(-\mathrm{bD})\} \quad (2)$$

where D^* and *F* are the perfusion-related diffusion coefficient and fraction, respectively; and *D* is the molecular diffusion coefficient. First, mono-exponential fitting was performed with b-values of 200 s/mm^2 and greater to obtain *D*. D^* and *F* were then derived from the bi-exponential function using Eq. (2) with all eight b-values.

Stretched exponential analysis with eight b-values was performed with the following equation:

$$S_b = S_0 \bullet \exp\{-(\mathrm{bDDC})^{\alpha}\} \quad (3)$$

where *DDC* is the distributed diffusion coefficient and *α* is the stretching parameter, which characterizes the deviation of the signal attenuation from the mono-exponential model. A value close to one indicates high homogeneity in apparent diffusion, whereas a low-value result from the non-exponential model is caused by the addition of multiple components.

Three permeability parameter maps, (volume transfer rate constant (K^{trans}), back flow rate constant (K_{ep}), and extravascular extracellular space volume fraction (V_e)), were calculated based on the extended Tofts pharmacokinetic model, which in turn is derived from two separate compartments, the plasma space and the extravascular extracellular space.

2.6. Statistical analysis

All statistical tests were performed at the two-sided 5% significance level using SPSS for Windows v. 22.0 software (SPSS, Chicago, IL) and JMP v. 11.0.0 software (SAS, Cary, NC). The Mann–Whitney *U* test was used to compare all metrics including ADC_{mean}, $ADC_{0–25}$, $ADC_{skewness}$, and $ADC_{kurtosis}$ in ADC histogram analysis; *D* and *f* in IVIM; *DDC* and *α* in the stretched exponential model; and K^{trans}, K_{ep}, and V_e in blood vessel permeability parameters between GS = 3 + 3 tumors versus GS ≥ 3 + 4 tumors and GS ≤ 3 + 4 tumors versus GS ≥ 4 + 3 tumors. The area under the curve (AUC) of receiver-operating characteristic (ROC) analysis was used to assess the diagnostic performance of each metric. In the ROC analyses, the DeLong test was used to compare AUC between metrics. Furthermore, for discrimination between GS = 3 + 3 tumors versus GS ≥ 3 + 4 tumors, and GS ≤ 3 + 4 tumors versus GS ≥ 4 + 3 tumors, the optimal cutoff value of each metric was determined by Youden index, and sensitivity and specificity for the discrimination of tumor aggressiveness were calculated. Relationships between all metrics and tumor

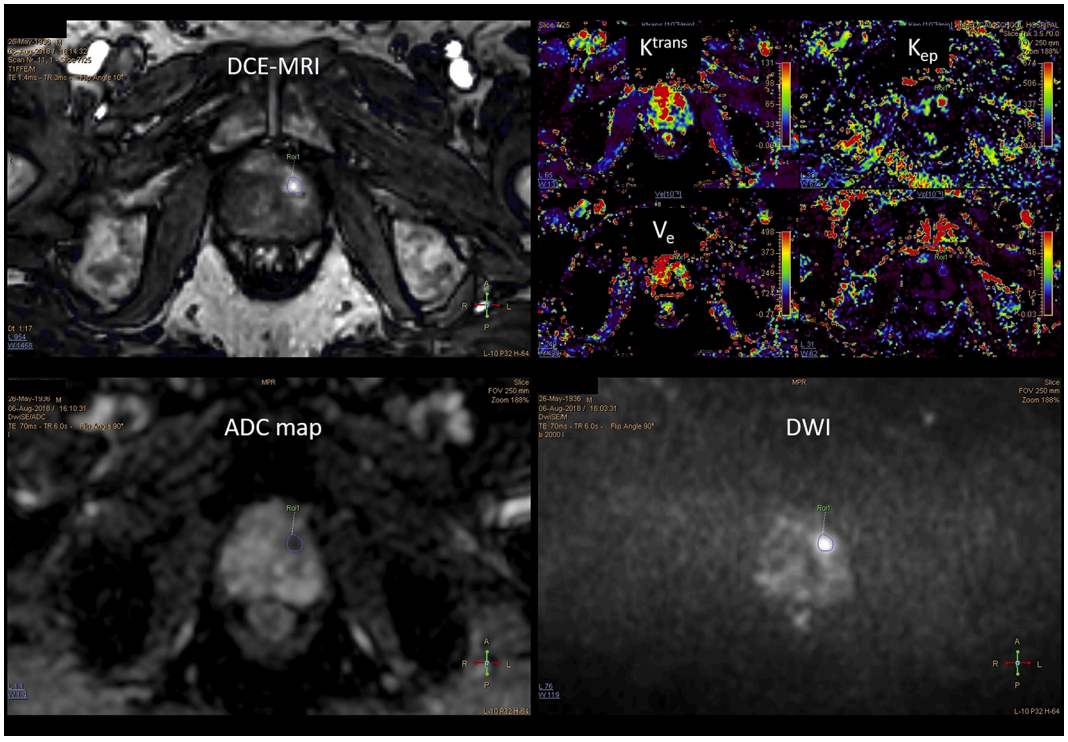

Fig. 2. Representative example of quantitative DCE-MRI analysis (permeability parameters: K^{trans}, K_{ep}, and V_e) of an 82-year-old man with cancer in the left peripheral zone (circle). The images were produced using a dedicated post-processing workstation (IntelliSpace Portal). DCE-MRI; dynamic contrast-enhanced MR imaging; ADC map: apparent diffusion coefficient map; DWI: diffusion-weighted imaging.

Gleason grade (GG; GG1, GS = 3 + 3; GG2, GS = 3 + 4; GG3, GS = 4 + 3; GG4, GS = 8; GG5, GS = 9 or 10) were assessed using Spearman's rank correlation coefficient (ρ) [16]. The Mann–Whitney *U* test and Spearman's rank correlation coefficient was performed using SPSS for Windows v. 22.0 software, and the ROC analysis with DeLong test, Youden index, and calculation of sensitivity and specificity was performed using JMP v. 11.0.0 software.

3. Results

3.1. PC characteristics

The dominant tumor was in the peripheral zone in 66/104 patients (63%), in the transition zone in 36/104 patients (35%), and in both the peripheral and transition zones in 2/104 patients (2%). The 104 PCs comprised GS = 3 + 3 in 15 tumors, GS = 3 + 4 in 32 tumors, GS = 4 + 3 in 28 tumors, GS = 4 + 4 in 21 tumors, and GS = 4 + 5 in 8 tumors. The GG distribution was GG1, $n = 15$; GG2, $n = 32$; GG3, $n = 28$; GG4, $n = 21$; and GG5, $n = 8$. The proportion of tumor visible on MRI was 100% (104/104) on DW images and 95% (87/92) on DCE images.

3.2. Comparison of ADC histogram analysis, IVIM, stretched exponential model, and permeability MRI for PC characterization

ADC_{mean}, $ADC_{0–25}$, *D*, *DDC*, and V_e were significantly lower and K_{ep} was significantly higher in GS ≥ 3 + 4 tumors than in GS = 3 + 3 tumors; also in GS ≥ 4 + 3 tumors than in GS ≤ 3 + 4 tumors ($P < 0.001$ to $P = 0.040$) (Table 1). However, there were no significant differences in $ADC_{skewness}$, $ADC_{kurtosis}$, *a*, and K^{trans} in both of these comparisons ($P = 0.302$ to $P = 0.996$) (Table 1). In contrast, *f* was significantly lower in GS ≥ 4 + 3 tumors than in GS ≤ 3 + 4 tumors ($P = 0.022$), but not significantly different between GS = 3 + 3 tumors and GS ≥ 3 + 4 tumors ($P = 0.514$) (Table 1). In ROC analysis, the AUC of the metrics ranged from 0.481 to 0.903 for separating GS = 3 + 3 tumors from GS ≥ 3 + 4 tumors, and from 0.485 to 0.916 for separating GS ≤ 3 + 4 tumors from GS ≥ 4 + 3 tumors (Table 2). The highest AUC was 0.903 in *D* for separating GS = 3 + 3 tumors from GS ≥ 3 + 4 tumors; and 0.916 in $ADC_{0–25}$ for separating GS ≤ 3 + 4 tumors from GS ≥ 4 + 3 tumors (Table 2). In metrics with AUC > 0.80, there were no significant differences between ADC_{mean} (0.884), $ADC_{0–25}$ (0.855), *D* (0.903), and *DDC* (0.868) for separating GS = 3 + 3 tumors from GS ≥ 3 + 4 tumors ($P = 0.072$ to $P = 0.673$) (Table 3). There were significant differences in AUC between $ADC_{0–25}$ (0.916) and *D* (0.853), and *DDC* (0.860) for separating GS ≤ 3 + 4 tumors from GS ≥ 4 + 3 tumors ($P = 0.040$ and $P = 0.022$, respectively) (Table 4). There was no significant difference between $ADC_{0–25}$ (0.916) and ADC_{mean} (0.885) ($P = 0.070$); or among ADC_{mean} (0.885), *D* (0.853), and *DDC* (0.860) ($P = 0.146$ to $P = 0.839$) (Table 4). For the discrimination of PC tumor aggressiveness at the optimal cutoff point by Youden index, the highest Youden index was 0.74 in *D* with an optimal cutoff point of 0.71×10^{-3} mm^2/s, sensitivity of 80.9%, and specificity of 93.3% for separating GS = 3 + 3 tumors from GS ≥ 3 + 4 tumors; and 0.63 in $ADC_{0–25}$ with optimal cutoff point of 0.61×10^{-3} mm^2/s, sensitivity of 93.0%, and specificity of 70.2% for separating GS ≤ 3 + 4 tumors from GS ≥ 4 + 3 tumors (Table 5).

Table 2
ADC with histogram analysis, IVIM, stretched exponential model, and DCE-MRI with permeability MRI: AUC for Discrimination of Tumor Aggressiveness and Correlation Coefficient with Gleason Grade.

Metric	GS = 3 + 3 vs. GS ≥ 3 + 4	GS ≤3 + 4 vs. GS ≥4 + 3	Correlation with Gleason grade (GG)[a]	
	AUC	AUC	ρ	P value
ADC_{mean}	0.8840	0.8848	−0.585	< 0.001
$ADC_{0–25}$	0.8554	0.9155	−0.627	< 0.001
$ADC_{Skewness}$	0.5879	0.5833	0.091	0.358
$ADC_{Kurtosis}$	0.4909	0.4848	0.095	0.337
D	0.9030	0.8533	−0.559	< 0.001
f	0.5567	0.6624	−0.240	0.014
DDC	0.8684	0.8600	−0.593	< 0.001
a	0.5818	0.5224	−0.013	0.899
K^{trans}	0.4805	0.5555	−0.075	0.479
K_{ep}	0.7100	0.6245	0.210	0.045
V_e	0.7039	0.6417	−0.231	0.027

Note- ADC: apparent diffusion coefficient; IVIM: intravoxel incoherent motion; DCE-MRI: dynamic contrast-enhanced MR imaging; AUC: area under the curve; GS: Gleason score; 0–25: 0–25th percentile; *D*: diffusion coefficient of slow decay; *f*: perfusion fraction; *DDC*: distributed diffusion coefficient; K^{trans}: volume transfer rate constant; K_{ep}: back flow rate constant; V_e: extravascular extracellular space volume fraction.

[a] Gleason grade (GG1, GS = 3 + 3; GG2, GS = 3 + 4; GG3, GS = 4 + 3; GG4, GS = 8; GG5, GS = 9 or 10).

Table 1
Summary of metrics in ADC with histogram analysis, IVIM, stretched exponential model, and DCE-MRI with permeability MRI between GS = 3 + 3 Tumors vs. GS ≥ 3 + 4 Tumors, and GS ≤ 3 + 4 Tumors vs. GS ≥ 4 + 3 Tumors.

Metric	GS = 3 + 3 (*n* = 15)		GS ≥ 3 + 4 (*n* = 89)		*P* value	GS ≤ 3 + 4 (*n* = 47)		GS ≥ 4 + 3 (*n* = 57)		P value
	Mean	SD	Mean	SD		Mean	SD	Mean	SD	
ADC_{mean} ($\times 10^{-3}$ mm^2/s)	0.89	0.19	0.63	0.14	< 0.001	0.77	0.18	0.59	0.11	< 0.001
$ADC_{0–25}$ ($\times 10^{-3}$ mm^2/s)	0.78	0.19	0.54	0.15	< 0.001	0.69	0.17	0.48	0.11	< 0.001
$ADC_{Skewness}$	0.11	0.72	0.39	0.57	0.302	0.26	0.61	0.43	0.59	0.352
$ADC_{Kurtosis}$	2.78	0.61	2.94	1.15	0.996	2.81	0.68	3.01	1.33	0.899
D ($\times 10^{-3}$ mm^2/s)	1.00	0.29	0.61	0.20	< 0.001	0.80	0.29	0.55	0.14	< 0.001
F (%)	20.3	11.9	18.3	9.67	0.514	20.9	10.4	16.7	9.26	0.022
DDC ($\times 10^{-3}$ mm^2/s)	1.42	0.57	0.81	0.32	< 0.001	1.13	0.49	0.71	0.21	< 0.001
a	0.71	0.10	0.69	0.11	0.367	0.69	0.09	0.69	0.12	0.992

Metric	GS = 3 + 3 (n = 15)		GS ≥ 3 + 4 (*n*=77)		P value	GS ≤ 3 + 4 (*n* = 42)		GS ≥ 4 + 3 (*n* = 50)		P value
	Mean	SD	Mean	SD		Mean	SD	Mean	SD	
K^{trans} ($\times 10^{-3}$/min)	135.7	97.0	138.1	126.6	0.812	147.8	122.1	129.3	122.1	0.361
K_{ep} ($\times 10^{-3}$/min)	470.8	255.7	727.8	361.3	0.010	590.5	299.0	766.1	386.0	0.040
V_e ($\times 10^{-3}$)	319.6	243.0	202.3	184.1	0.013	287.4	249.0	166.0	119.1	0.020

Note- ADC: apparent diffusion coefficient; IVIM: intravoxel incoherent motion; DCE-MRI: dynamic contrast-enhanced MR imaging; GS: Gleason score; SD: standard deviation; 0–25: 0–25th percentile; *D*: diffusion coefficient of slow decay; *f*: perfusion fraction; *DDC*: distributed diffusion coefficient; K^{trans}: volume transfer rate constant; K_{ep}: back flow rate constant; V_e: extravascular extracellular space volume fraction.

Table 3
Comparison of AUC for discrimination of GS = 3 + 3 Tumors vs. GS ≥ 3 + 4 Tumors between Metrics of ADC with Histogram Analysis, IVIM, Stretched Exponential Model, and DCE-MRI with Permeability MRI.

Metric	$ADC_{0–25}$	$ADC_{Skewness}$	$ADC_{Kurtosis}$	*D*	*f*	*DDC*	*a*	K^{trans}	K_{ep}	V_e
ADC_{mean}	0.326	0.002*	< 0.001*	0.253	0.001*	0.167	0.001*	< 0.001*	0.013*	0.082
$ADC_{0–25}$	–	0.003*	< 0.001*	0.165	0.003*	0.673	0.006*	< 0.001*	0.049*	0.155
$ADC_{Skewness}$	–	–	0.330	0.001*	0.806	0.003*	0.964	0.328	0.288	0.355
$ADC_{Kurtosis}$	–	–	–	< 0.001*	0.503	< 0.001*	0.445	0.919	0.030*	0.034*
D	–	–	–	–	< 0.001*	0.072	< 0.001*	< 0.001*	0.007*	0.053
f	–	–	–	–	–	0.002*	0.859	0.343	0.144	0.283
DDC	–	–	–	–	–	–	0.003*	< 0.001*	0.0027*	0.121
a	–	–	–	–	–	–	–	0.335	0.115	0.244
K^{trans}	–	–	–	–	–	–	–	–	< 0.001*	0.100
K_{ep}	–	–	–	–	–	–			–	0.953

Note- AUC: area under the curve; GS: Gleason score; ADC: apparent diffusion coefficient; IVIM: intravoxel incoherent motion; DCE-MRI: dynamic contrast-enhanced MR imaging; 0–25: 0–25th percentile; *D*: diffusion coefficient of slow decay; *f*: perfusion fraction; *DDC*: distributed diffusion coefficient; K^{trans}: volume transfer rate constant; K_{ep}: back flow rate constant; V_e: extravascular extracellular space volume fraction.
The numbers in Table are P value. The * indicates P value <0.05.

Table 4
Comparison of AUC for discrimination of GS ≤ 3 + 4 Tumors vs. GS ≥ 4 + 3 Tumors between metrics of ADC with histogram analysis, IVIM, stretched exponential model, and DCE-MRI with permeability MRI.

Metric	$ADC_{0–25}$	$ADC_{Skewness}$	$ADC_{Kurtosis}$	*D*	*f*	*DDC*	*a*	K^{trans}	K_{ep}	V_e
ADC_{mean}	0.070	< 0.001*	< 0.001*	0.244	< 0.001*	0.146	< 0.001*	< 0.001*	< 0.001*	< 0.001*
$ADC_{0–25}$	–	< 0.001*	< 0.001*	0.040*	< 0.001*	0.022*	< 0.001*	< 0.001*	< 0.001*	< 0.001*
$ADC_{Skewness}$	–	–	0.092	< 0.001*	0.359	< 0.001*	0.496	0.752	0.590	0.504
$ADC_{Kurtosis}$	–	–	–	< 0.001*	0.023*	< 0.001*	0.670	0.450	0.078	0.085
D	–	–	–	–	0.005*	0.839	< 0.001*	< 0.001*	< 0.001*	0.002*
f	–	–	–	–	–	< 0.001*	0.006*	0.253	0.649	0.825
DDC	–	–	–	–	–	–	< 0.001*	< 0.001*	< 0.001*	0.004*
a	–	–	–	–	–	–	–	0.704	0.280	0.192
K^{trans}	–	–	–	–	–	–	–	–	0.502	0.024*
K_{ep}	–	–	–	–	–	–			–	0.836

Note- AUC: area under the curve; GS: Gleason score; ADC: apparent diffusion coefficient; IVIM: intravoxel incoherent motion; DCE-MRI: dynamic contrast-enhanced MR imaging; 0–25: 0–25th percentile; *D*: diffusion coefficient of slow decay; *f*: perfusion fraction; *DDC*: distributed diffusion coefficient; K^{trans}: volume transfer rate constant; K_{ep}: back flow rate constant; V_e: extravascular extracellular space volume fraction.
The numbers in Table are P value. The * indicates P value <0.05.

Table 5
ADC with histogram analysis, IVIM, stretched exponential model, and DCE-MRI with permeability MRI: Optimal Cutoff Values, Diagnostic Sensitivity, and Diagnostic Specificity for Discrimination of Tumor Aggressiveness.

Metric	GS = 3 + 3 vs. GS ≥ 3 + 4				GS ≤3 + 4 vs. GS ≥4 + 3			
	Youden index	Cutoff value	Sensitivity (%)	Specificity (%)	Youden index	Cutoff value	Sensitivity (%)	Specificity (%)
ADC_{mean} ($\times 10^{-3}$ mm^2/s)	0.67	0.81	93.3	73.3	0.58	0.69	89.5	68.1
$ADC_{0–25}$ ($\times 10^{-3}$ mm^2/s)	0.62	0.74	95.5	66.7	0.63	0.61	93.0	70.2
$ADC_{Skewness}$	0.21	−0.37	94.4	26.7	0.14	−0.22	93.0	21.3
$ADC_{Kurtosis}$	0.17	3.80	16.9	100	0.15	3.45	29.8	85.1
D ($\times 10^{-3}$ mm^2/s)	0.74	0.71	80.9	93.3	0.48	0.68	84.2	63.8
F (%)	0.20	15.5	40.5	80.0	0.26	15.4	47.4	78.7
DDC ($\times 10^{-3}$ mm^2/s)	0.64	1.04	84.3	80.0	0.57	0.79	71.9	85.1
a	0.20	0.79	86.5	33.3	0.11	0.81	17.5	93.6
K^{trans} ($\times 10^{-3}$/min)	0.17	180.3	29.9	86.7	0.13	262.8	94.0	19.1
K_{ep} ($\times 10^{-3}$/min)	0.34	528.4	67.5	53.3	0.23	545.6	70.0	52.4
V_e ($\times 10^{-3}$)	0.40	149.3	53.3	86.7	0.33	177.2	66.0	66.7

Note- ADC: apparent diffusion coefficient; IVIM: intravoxel incoherent motion; DCE-MRI: dynamic contrast-enhanced MR imaging; 0–25: 0–25th percentile; *D*: diffusion coefficient of slow decay; *f*: perfusion fraction; *DDC*: distributed diffusion coefficient; K^{trans}: volume transfer rate constant; K_{ep}: back flow rate constant; V_e: extravascular extracellular space volume fraction.

3.3. Correlations between all metrics and GG

$ADC_{0–25}$ correlated most strongly with GG ($\rho = -0.627$, $P < 0.001$) (Table 2).

4. Discussion

For discrimination between GS = 3 + 3 tumors and GS ≥ 3 + 4 tumors, although *D* had the highest AUC, there were no significant differences among metrics with AUC > 0.80, including ADC_{mean}, $ADC_{0–25}$, *D*, and *DDC*. In addition, *D* had the highest Youden index, with sensitivity of 80.9% and specificity of 93.3%. In assessment of the aggressiveness of PC tumors in the clinical setting, however, it may be preferable to use a metric with high sensitivity rather than high specificity; for the reason that underestimation of tumor aggressiveness risks serious clinical negligence in terms of the opportunity for curative therapy such as radical prostatectomy, and may affect the prognosis of the patient. In that sense, metrics such as ADC_{mean} (sensitivity = 93.3%) and $ADC_{0–25}$ (sensitivity =

95.5%) with higher sensitivity and acceptable AUC, Youden index, and specificity are considered suitable for clinical application.

For discrimination between GS $\leq 3 + 4$ tumors and GS $\geq 4 + 3$ tumors, the AUC of $ADC_{0–25}$ was highest among all metrics, and was significantly higher than those of *D* and *DDC*. $ADC_{0–25}$ had the highest Youden index, with sensitivity of 93.0% and specificity of 70.2%, and the best correlation with GG ($\rho = -0.627$). These results suggest that $ADC_{0–25}$ is a more reliable predictive metric for discrimination of tumor aggressiveness in PC for the two outcomes compared with IVIM and stretched exponential model, and permeability MRI. In particular, the benefit of the histogram metric using lower ADC regions (pixels) such as 0–25th percentile of ADC may relate to its sensitivity to more aggressive sub-regions within a heterogeneous tumor in PC [17,18], which may not be appreciated using conventional metrics because of volume averaging. However, to improve the reduction in specificity that is the trade-off for high sensitivity via the clinical use of mono-exponential model ADC with histogram analysis (such as $ADC_{0–25}$), it will be necessary to consider solutions that can be applied in combination with clinical information, such as PSA density (PSAD), prostate cancer antigen 3 (PCA3), Prostate Health Index (PHI), and four kallikrein (4 K) score [13].

A number of investigations have reported comparable diagnostic performance of PC risk stratification between IVIM (mainly *D*) and mono-exponential model ADC [19–24]; whereas only one study has observed better performance of *D* in IVIM compared with mono-exponential model ADC [25]. In contrast, almost all previous studies have shown insufficient diagnostic performance of *f* in IVIM [21,23–25]. Similarly, the diagnostic capabilities of the stretched exponential model (mainly *DDC*) for risk stratification of PC tend to be similar to that of mono-exponential ADC [9,26,27]. Several investigators have reported that this equivalence of diagnostic performance for assessment of tumor aggressiveness may be due to strong correlations between these metrics, or between GS and these metrics, which may suggest that these metrics individually provide similar information in PC [9,20–22,26].

In the present study, the diagnostic performance of tumor aggressiveness using DCE-MRI with permeability MRI was relatively low compared with quantitative DWI metrics. Other than the study by Cho et al., which had a small sample size [28], most past studies have reported a lower correlation between permeability metrics and GS compared with than that between quantitative DWI metrics and GS [12,29–32]. As a cause of low correlation between permeability metrics and GS, not all csPCs show enhancement on DCE-MRI [33,34]. In addition, permeability metrics and enhancement effect on DCE-MRI showed a significant difference only between low-to-intermediate risk tumors and high-risk tumors such as GS $\geq 4 + 4$, which suggests that neovascularization in PC may develop rapidly in high-risk tumors [33,35]. According to previous investigations of the management of patients with PC, qualitative and quantitative DCE-MRI should be used for detection of local recurrence following treatment such as radical prostatectomy or radiotherapy, and for determination of therapeutic effect and prognostic prediction, rather than for assessment of tumor aggressiveness [34,36].

Some limitations exist in our study. First, the study had a relatively small sample size, was retrospective in design, and was performed at a single center. Therefore, further prospective multi-center studies with a larger number of patients are needed to validate the present results. Second, the reference standard for pathological evaluation was cognitive MRGB in 25/104 (24%) patients. Tumor GS obtained from cognitive biopsy may have been underestimated compared with that from MRFGB or total prostatectomy. Third, we performed quantitative evaluation using a 2D ROI placement technique, but it might be preferable to use a whole-lesion 3D volume of interest (VOI) measurement for assessing heterogeneous nature within a PC lesion. However, a recent study revealed no improvement in intrareader or interreader reproducibility, or diagnostic performance for prostate ADC measurements using a 3D VOI compared with a 2D ROI [37]. Therefore, 2D ROI measurement, which is simpler than 3D VOI measurement, will accelerate the clinical application of quantitative DWI for assessment of risk stratification in the clinical management of patients with PC.

5. Conclusions

The present observations using quantitative DWI with b-values up to 2000 s/mm^2 and DCE-MRI showed no apparent clinical superiority for assessment of tumor aggressiveness in PC of recently proposed methods such as non-Gaussian models (including IVIM and stretched exponential model) or quantitative DCE-MRI with permeability MRI over the mono-exponential model with histogram analysis. Although mono-exponential ADC with histogram analysis may be a reliable predictor of risk stratification of PC, further improvements in diagnostic specificity will be essential for its clinical application.

Funding statement

This research did not receive any specific grant from funding agencies in the public, commercial, or not-for-profit sectors.

Declaration of Competing Interest

The authors have no conflicts of interest to disclose.

References

[1] Sonn GA, Margolis DJ, Marks LS. Target detection: magnetic resonance imaging-ultrasound fusion-guided prostate biopsy. Urol Oncol 2014;32:903–11. https://doi.org/10.1016/j.urolonc.2013.08.006.
[2] Rajinikanth A, Manoharan M, Soloway CT, Civantos FJ, Soloway MS. Trends in Gleason score: concordance between biopsy and prostatectomy over 15 years. Urology. 2008;72:177–82. https://doi.org/10.1016/j.urology.2007.10.022.
[3] Tamada T, Sone T, Jo Y, Yamamoto A, Ito K. Diffusion-weighted MRI and its role in prostate cancer. NMR Biomed 2014;27:25–38. https://doi.org/10.1002/nbm.2956.
[4] Donati OF, Mazaheri Y, Afaq A, Vargas HA, Zheng J, Moskowitz CS, et al. Prostate cancer aggressiveness: assessment with whole-lesion histogram analysis of the apparent diffusion coefficient. Radiology. 2014;271:143–52. https://doi.org/10.1148/radiol.13130973.
[5] Tamada T, Prabhu V, Li J, Babb JS, Taneja SS, Rosenkrantz AB. Prostate cancer: diffusion-weighted MR imaging for detection and assessment of aggressiveness-comparison between conventional and kurtosis models. Radiology. 2017;284:100–8. https://doi.org/10.1148/radiol.2017162321.
[6] Rosenkrantz AB, Padhani AR, Chenevert TL, Koh DM, De Keyzer F, Taouli B, et al. Body diffusion kurtosis imaging: basic principles, applications, and considerations for clinical practice. J Magn Reson Imaging 2015;42:1190–202. https://doi.org/10.1002/jmri.24985.
[7] Le Bihan D, Breton E, Lallemand D, Aubin ML, Vignaud J, Laval-Jeantet M. Separation of diffusion and perfusion in intravoxel incoherent motion MR imaging. Radiology. 1988;168:497–505. https://doi.org/10.1002/jmri.24985.
[8] Le Bihan D, Breton E, Lallemand D, Grenier P, Cabanis E, Laval-Jeantet M. MR imaging of intravoxel incoherent motions: application to diffusion and perfusion in neurologic disorders. Radiology. 1986;161:401–7. https://doi.org/10.1148/radiology.161.2.3763909.
[9] Toivonen J, Merisaari H, Pesola M, Taimen P, Boström PJ, Pahikkala T, et al. Mathematical models for diffusion-weighted imaging of prostate cancer using b-values up to 2000 s/mm(2): correlation with Gleason score and repeatability of region of interest analysis. Magn Reson Med 2015;74:1116–24. https://doi.org/10.1002/mrm.25482.
[10] Singanamalli A, Rusu M, Sparks RE, Shih NN, Ziober A, Wang LP, et al. Identifying in vivo DCE MRI markers associated with microvessel architecture and Gleason grades of prostate cancer. J Magn Reson Imaging 2016;43:149–58. https://doi.org/10.1002/jmri.24975.
[11] Vos EK, Litjens GJ, Kobus T, Hambrock T, Hulsbergen-van de Kaa CA, Barentsz JO, et al. Assessment of prostate cancer aggressiveness using dynamic contrast-enhanced magnetic resonance imaging at 3 T. Eur Urol 2013;64:448–55. https://doi.org/10.1016/j.eururo.2013.05.045.
[12] Oto A, Yang C, Kayhan A, Tretiakova M, Antic T, Schmid-Tannwald C, et al. Diffusion-weighted and dynamic contrast-enhanced MRI of prostate cancer: correlation of quantitative MR parameters with Gleason score and tumor angiogenesis. AJR Am J Roentgenol 2011;197:1382–90. https://doi.org/10.2214/AJR.11.6861.
[13] Rosenkrantz AB, Verma S, Choyke P, Eberhardt SC, Eggener SE, Gaitonde K, et al. Prostate magnetic resonance imaging and magnetic resonance imaging targeted biopsy in patients with a prior negative biopsy: a consensus statement by AUA and SAR. J Urol 2016;196:1613–8. https://doi.org/10.1016/j.juro.2016.06.079.
[14] Tamada T, Kido A, Yamamoto A, Takeuchi M, Miyaji Y, Moriya T, et al. Comparison of biparametric and multiparametric mri for clinically significant

prostate cancer detection with PI-RADS version 2.1. J Magn Reson Imaging 2021; 53:283–91. https://doi.org/10.1002/jmri.27283.
[15] Tamada T, Sone T, Higashi H, Jo Y, Yamamoto A, Kanki A, et al. Prostate cancer detection in patients with total serum prostate-specific antigen levels of 4-10 ng/mL: diagnostic efficacy of diffusion-weighted imaging, dynamic contrast-enhanced MRI, and T2-weighted imaging. AJR Am J Roentgenol 2011;197:664–70. https://doi.org/10.2214/AJR.10.5923.
[16] Epstein JI, Egevad L, Amin MB, Delahunt B, Srigley JR, Humphrey PA, et al. The 2014 International Society of Urological Pathology (ISUP) Consensus Conference on gleason grading of prostatic carcinoma: definition of grading patterns and proposal for a new grading system. Am J Surg Pathol 2016;40:244–52. https://doi.org/10.1097/PAS.0000000000000530.
[17] Rosenkrantz AB, Ream JM, Nolan P, Rusinek H, Deng FM, Taneja SS. Prostate cancer: utility of whole-lesion apparent diffusion coefficient metrics for prediction of biochemical recurrence after radical prostatectomy. AJR Am J Roentgenol 2015; 205:1208–14. https://doi.org/10.2214/AJR.15.14482.
[18] Donati OF, Mazaheri Y, Afaq A, Vargas HA, Zheng J, Moskowitz CS, et al. Prostate cancer aggressiveness: assessment with whole-lesion histogram analysis of the apparent diffusion coefficient. Radiology. 2014;271:143–52. https://doi.org/10.1148/radiol.13130973.
[19] Bao J, Wang X, Hu C, Hou J, Dong F, Guo L. Differentiation of prostate cancer lesions in the transition zone by diffusion-weighted MRI. Eur J Radiol Open 2017; 4:123–8. https://doi.org/10.1016/j.ejro.2017.08.003.
[20] Shan Y, Chen X, Liu K, Zeng M, Zhou J. Prostate cancer aggressive prediction: preponderant diagnostic performances of intravoxel incoherent motion (IVIM) imaging and diffusion kurtosis imaging (DKI) beyond ADC at 3.0 T scanner with Gleason score at final pathology. Abdom Radiol (NY) 2019;44:3441–52. https://doi.org/10.1007/s00261-019-02075-3.
[21] Yang DM, Kim HC, Kim SW, Jahng GH, Won KY, Lim SJ, et al. Prostate cancer: correlation of intravoxel incoherent motion MR parameters with Gleason score. Clin Imaging 2016;40:445–50. https://doi.org/10.1016/j.clinimag.2016.01.001.
[22] Merisaari H, Movahedi P, Perez IM, Toivonen J, Pesola M, Taimen P, et al. Fitting methods for intravoxel incoherent motion imaging of prostate cancer on region of interest level: repeatability and Gleason score prediction. Magn Reson Med 2017; 77:1249–64. https://doi.org/10.1002/mrm.26169.
[23] Barbieri S, Brönnimann M, Boxler S, Vermathen P, Thoeny HC. Differentiation of prostate cancer lesions with high and with low Gleason score by diffusion-weighted MRI. Eur Radiol 2017;27:1547–55. https://doi.org/10.1007/s00330-016-4449-5.
[24] Valerio M, Zini C, Fierro D, Giura F, Colarieti A, Giuliani A, et al. 3T multiparametric MRI of the prostate: does intravoxel incoherentmotion diffusion imaging have a role in the detection andstratification of prostate cancer in the peripheral zone? Eur J Radiol 2016;85:790–4. https://doi.org/10.1016/j.ejrad.2016.01.006.
[25] Zhang YD, Wang Q, Wu CJ, Wang XN, Zhang J, Liu H, et al. The histogram analysis of diffusion-weighted intravoxel incoherent motion (IVIM) imaging for differentiating the Gleason grade of prostate cancer. Eur Radiol 2015;25: 994–1004. https://doi.org/10.1007/s00330-014-3511-4.
[26] Liu W, Liu XH, Tang W, Gao HB, Zhou BN, Zhou LP. Histogram analysis of stretched-exponential and monoexponential diffusion-weighted imaging models for distinguishing low and intermediate/high Gleason scores in prostate carcinoma. J Magn Reson Imaging 2018;48:491–8. https://doi.org/10.1002/jmri.25958.
[27] Kim E, Kim CK, Kim HS, Jang DP, Kim IY, Hwang J. Histogram analysis from stretched exponential model on diffusion-weighted imaging: evaluation of clinically significant prostate cancer. Br J Radiol 2020;935:20190757. https://doi.org/10.1259/bjr.20190757.
[28] Cho E, Chung DJ, Yeo DM, Sohn D, Son Y, Kim T, et al. Optimal cut-off value of perfusion parameters for diagnosing prostate cancer and for assessing aggressiveness associated with Gleason score. Clin Imaging 2015;39:834–40. https://doi.org/10.1016/j.clinimag.2015.04.020.
[29] Ma XZ, Lv K, Sheng JL, Yu YX, Pang PP, Xu MS, et al. Application evaluation of DCE-MRI combined with quantitative analysis of DWI for the diagnosis of prostate cancer. Oncol Lett 2019;17:3077–84. https://doi.org/10.3892/ol.2019.9988.
[30] Vos EK, Litjens GJ, Kobus T, Hambrock T, Hulsbergen-van de Kaa CA, Barentsz JO, et al. Assessment of prostate cancer aggressiveness using dynamic contrast-enhanced magnetic resonance imaging at 3 T. Eur Urol 2013;64:448–55. https://doi.org/10.1016/j.eururo.2013.05.045.
[31] Sanz-Requena R, Martí-Bonmatí L, Pérez-Martínez R, García-Martí G. Dynamic contrast-enhanced case-control analysis in 3T MRI of prostate cancer can help to characterize tumor aggressiveness. Eur J Radiol 2016;85:2119–26. https://doi.org/10.1016/j.ejrad.2016.09.022.
[32] Oto A, Kayhan A, Jiang Y, Tretiakova M, Yang C, Antic T, et al. Prostate cancer: differentiation of central gland cancer from benign prostatic hyperplasia by using diffusion-weighted and dynamic contrast-enhanced MR imaging. Radiology. 2010; 257:715–23. https://doi.org/10.1148/radiol.10100021.
[33] Kido A, Tamada T, Kanomata N, Yamamoto A, Miyaji Y, Nagai A, et al. Multidimensional analysis of clinicopathological characteristics of false-negative clinically significant prostate cancers on multiparametric MRI of the prostate in Japanese men. Jpn J Radiol 2019;37:154–64. https://doi.org/10.1007/s11604-018-0801-9.
[34] Muglia VF, Reis RB, Rocha TO, Silva AR, Noworolski S, Westphalen AC. Hypoenhancing prostate cancers on dynamic contrast-enhanced MRI are associated with poor outcomes in high-risk patients: results of a hypothesis generating study. Abdom Radiol (NY) 2019;44:723–31. https://doi.org/10.1007/s00261-018-1771-1.
[35] Hötker AM, Mazaheri Y, Aras Ö, Zheng J, Moskowitz CS, Gondo T, et al. Assessment of prostate cancer aggressiveness by use of the combination of quantitative DWI and dynamic contrast-enhanced MRI. AJR Am J Roentgenol 2016;206:756–63. https://doi.org/10.2214/AJR.15.14912.
[36] Alonzi R, Padhani AR, Taylor NJ, Collins DJ, D'Arcy JA, Stirling JJ, et al. Antivascular effects of neoadjuvant androgen deprivation for prostate cancer: an in vivo human study using susceptibility and relaxivity dynamic MRI. Int J Radiat Oncol Biol Phys 2011;80:721–7. https://doi.org/10.1016/j.ijrobp.2010.02.060.
[37] Tamada T, Huang C, Ream JM, Taffel M, Taneja SS, Rosenkrantz AB. Apparent diffusion coefficient values of prostate cancer: comparison of 2D and 3D ROIs. AJR Am J Roentgenol 2018;210:113–7. https://doi.org/10.2214/AJR.17.18495.